High-temperature elastic moduli of bulk nanostructured *n*- and *p*-type silicon germanium

J. R. Gladden,[1] G. Li,[1] R. Adebisi,[1] S. Firdosy,[2] T. Caillat,[2] and V. Ravi[2,3]
[1]*Department of Physics and Astronomy, University of Mississippi, University, Mississippi 38677, USA*
[2]*Jet Propulsion Laboratory, California Institute of Technology, 4800 Oak Grove Drive, Pasadena, California 91109, USA*
[3]*California State Polytechnic University, 3801 W. Temple Avenue, Pomona, California 91768, USA*
(Received 22 June 2010; published 30 July 2010)

Resonant ultrasound spectroscopy (RUS) has been used to measure the elastic moduli of *n*- and *p*-type doped polycrystalline bulk nanostructured silicon germanium alloys at elevated temperatures. A direct contact RUS transducer system with a working temperature range up to 900 K was successfully constructed for these measurements. For higher temperatures (up to 1300 K), we employed a traditional buffer rod RUS system. Experimental results show the Young's and shear moduli of *p*-type SiGe alloys monotonically decrease with increasing temperatures in the 300–1200 K range. The *n*-type samples show a marked stiffening beginning at 675 K which does not repeat upon cooling or subsequent reheating. We attribute the stiffening of the *n*-type samples to the thermally activated precipitation of the phosphorous dopant. Electrical resistivity and Seebeck coefficient data are also presented for both types of SiGe which support this conclusion.

DOI: 10.1103/PhysRevB.82.045209 PACS number(s): 81.40.Jj, 61.72.uf, 62.65.+k, 72.20.Pa

I. INTRODUCTION

Alternative methods to generate electric power without carbon emissions are an increasingly important, even vital, area of research. One such method is solid-state thermoelectric (TE) devices, in which thermal gradients produce electric potentials. One of the crucial challenges confronting this field is increasing the fundamental material thermoelectric efficiency, as quantified by the figure of merit: $ZT=\frac{\sigma S^2 T}{\kappa_T}$, where T is the absolute temperature, σ is electrical conductivity, S is the thermopower, and κ_T is the total thermal conductivity. In the past several decades, many researchers have been actively searching for high-performance thermoelectric materials that could be used for waste heat-recovery applications and, of particular interest to the Jet Propulsion Laboratory (JPL), in power generators on deep-space probes.[1] Silicon germanium (SiGe) alloys have been used in radioisotope thermoelectric generators (RTGs) to power several U.S. spacecraft.[2,3] They can be doped *p*- and *n*-type and are capable of operating over long periods of time at temperatures up to 1273 K. A new generation of bulk nanostructured SiGe alloys has been developed over the last several years at JPL and efforts are in progress to study their integration into advanced RTGs. In addition to the figure of merit and associated properties, temperature-dependent mechanical properties are critical to ensure that the stress and vibration levels experienced by the SiGe materials and thermoelectric couples during launch and cruise will remain safely below fracture loads. Thermomechanical characterization[4,5] of a range of thermoelectric materials has been undertaken at JPL as a key component of device development to determine the thermomechanical properties of advanced TE materials. As part of an effort to determine the temperature dependence of the mechanical properties of nanostructured bulk SiGe materials, elastic moduli were measured using a resonant ultrasound spectroscopy (RUS) technique.

RUS is an elegant and efficient method of obtaining the full elastic tensor and acoustic attenuation of a solid material. RUS in its modern form was introduced in 1991 and developed over the course of that decade.[6–10] Several more recent review papers and books have also been published.[11–13] In a RUS measurement, a carefully polished parallelepiped sample is placed between two acoustic transducers with one driving the sample with a sinusoidal stress and the other detecting the sample response. Figure 1 shows a block diagram of the measurement. When the drive frequency matches a natural frequency of the sample, the displacement amplitude increases by roughly the quality factor ($Q=f_0/\Delta f$) of the resonance. The displacements for the first 15 normal modes of a parallelepiped of typical dimensions for a RUS sample are shown in Fig. 2 where nodal and antinodal regions are indicated by dark and light (red and yellow in color) regions, respectively. The resulting peaks in the frequency domain can then be fit with a Lorentzian line shape to extract the center frequencies and quality factors. An ordered list of these measured natural frequencies of the sample constitutes the vibrational spectrum. The measured spectrum is then compared to a spectrum computed from the known parameters of dimensions, density, and initial estimates for elastic constants, which are adjusted in a least-squares sense to best fit the measured data.

RUS has been widely used for room- and low-temperature measurements for a wide variety of materials. Applications in the high-temperature regime, however, have been limited,

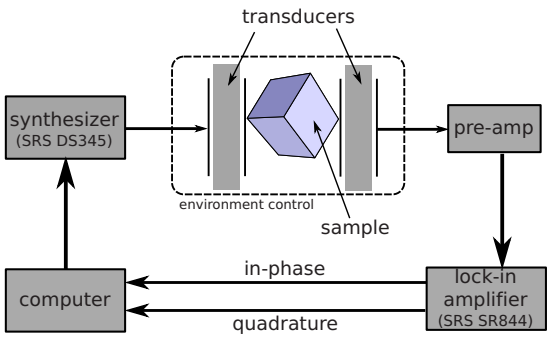

FIG. 1. (Color online) Block diagram for a RUS measurement.

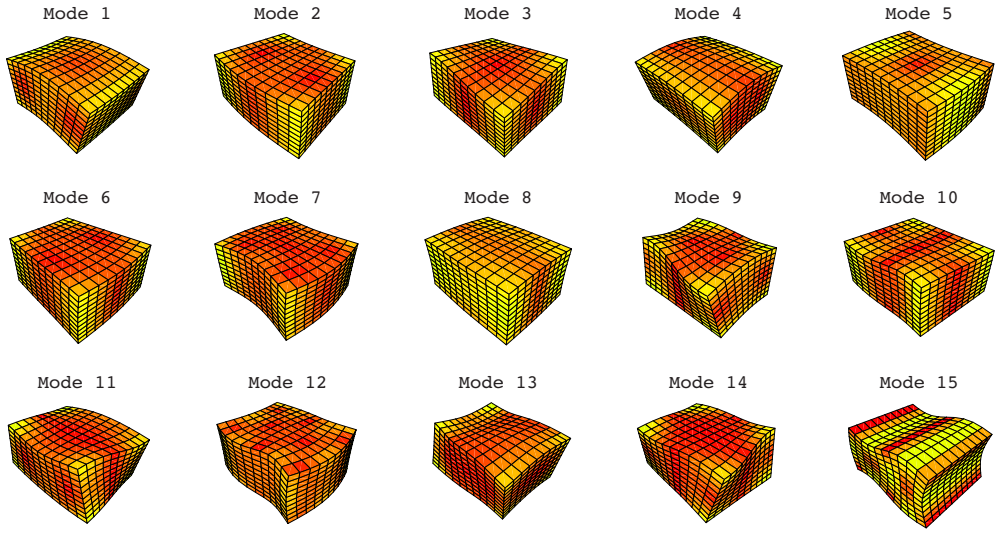

FIG. 2. (Color online) Surface displacements for the first 15 normals modes of a parallelepiped in order of increasing frequency. The darker (red in color) regions denote nodes and lighter (yellow in color) denote antinodes. Note the specific order of the modes types will vary somewhat depending on geometry and the amplitudes are greatly exaggerated.

partly due to the difficulties caused by the weak-resonance signals at high temperatures. High-temperature RUS methods have traditionally been implemented by separating the sample and the transducers with buffer rods (BRs) made of materials with low acoustic attenuation and good thermal stability such as ceramic alumina or fused quartz.[14,15]

II. MATERIALS AND METHODS

Two high-temperature RUS systems were designed for these experiments. The direct contact (DC) transducer system places gold-/chromium-coated lithium niobate ($LiNbO_3$) piezoelectric elements in direct contact with the sample under study. The electrical connections are made with conductive epoxy (Epo-Tek E2101) and electrical signals are carried by mineral-insulated coaxial cables (ThermoCoax, Inc.).[16] The direct contact system loses sensitivity near 900 K due to thermal activation of charge carriers in the $LiNbO_3$.[17] The BR system uses two fused quartz rods (diameter 3.125 mm and length 20 cm) as an acoustic waveguide between the sample in the hot zone and the piezoelectric elements. A comparison of resonance data acquired by the two systems for a particular sample at 680 K is shown in Fig. 3. This figure shows the much improved signal-to-noise ratio (SNR) of the DC system. While the reduced SNR of the BR system can be problematic, RUS is quite a robust experimental method in the sense that the only feature of each peak which affects the analysis is the center frequency (not, for instance, amplitude). As a case in point, the strong peak at about 1042 kHz in the DC data corresponds to the extremely small (yet still discernible) peak in the BR data at nearly the same frequency. Both these peaks were used in the fitted spectra. More problematic than the reduced SNR in the BR system are extra features in the resonance spectrum. These features are attributed to radial resonance modes of the buffer rods and need to be carefully separated from the sample peaks. The buffer rods have one dimension (length) that is much longer than the sample size (20 cm versus 0.2 cm) so that, in the frequency range of interest, the extensional and torsional modes for the buffer rods are of very high order. The peaks for these modes are therefore closely spaced enough to result in a roughly flat background (individual peaks cannot be resolved). However, the radial modes are independent of length meaning that low-order radial modes can exist in the low-order frequency ranges of typical RUS samples.[18] A third issue with the buffer rod system are loading effects induced by $\sim$10 g buffer rod. A controlled study of these effects showed that loading for our system upshifts particular modes by up to about 0.1% which is within typical frequency fit errors. Buffer rod loading effects motivate the acquisition of data by both DC and BR systems in their common temperature range (300–800 K) for direct comparison. Finally, to minimize oxidation, a low-flow ($\sim$1 lpm) inert gas (Ar) flushing system was used which maintained O_2 levels below 5 ppm inside the quartz tube furnace (Carbolite model MTF 12/38/250). Acquisition of acoustic data takes about 20 min at each temperature, during which temperature variations of about ± 0.5 K were observed. While the ramping rate is not linear, an average heating rate between temperatures where data were acquired is about 5.0 K/min for the DC system and 9.0 K/min for the BR system.

Nanopowders of SiGe materials were prepared by a ball milling technique. The powders were compacted into cylindrical samples using a uniaxial hot-pressing technique. The final sample compositions are: $Si_{0.784}Ge_{0.196}P_{0.020}$ for the *n*-type samples and $Si_{0.787}Ge_{0.197}B_{0.016}$ for the *p*-type samples. The samples had a density of about 99.5% of the theoretical density and the average crystallite size was determined by an x-ray technique and was found to be about 70 nm for the bulk nanostructured samples using the Scherrer formula. A low-speed diamond saw with Vernier displacement and rotation scales was used to cut the bars into precise smaller rectangular parallelepiped pieces. Each sample was then polished using diamond lapping paper. Typical final dimensions were between 2.5 and 4.0 mm on each side.

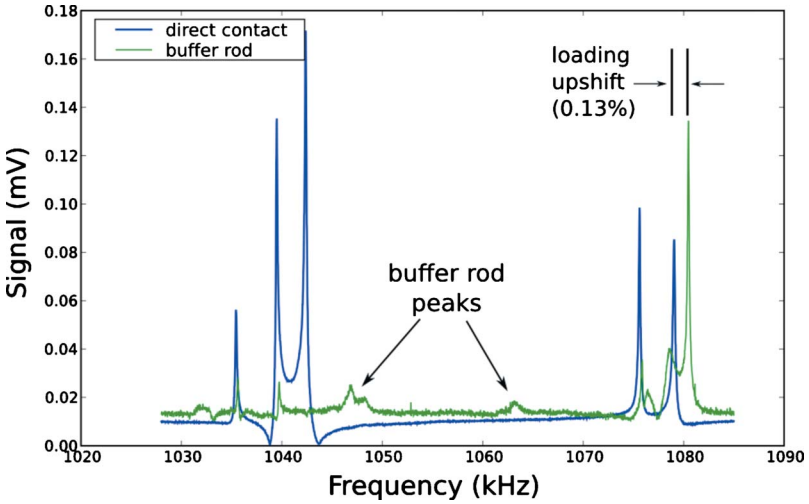

FIG. 3. (Color online) Frequency response data of a SiGe sample at 680 K obtained by the direct contact and buffer rod transduction systems. The buffer rod data have been amplified by a factor of 10.

Samples were ultrasonically cleaned in a sequence of acetone followed by ethanol baths prior to high-temperature measurements.

A complete temperature test up to 1300 K is typically a two-step process: the DC system is first used to take data from room temperature to about 900 K; and after the sample has cooled, it is removed and remounted on the BR system for measurements at higher temperatures, up to about 1300 K. In the temperature range already covered by the DC system, data are taken coarsely (every 100 or 200 K) to check consistency between the systems, loading effects, and to aid in buffer rod peak rejection (see Fig. 3). A waiting time of 10 min is necessary for the sample to reach equilibrium internally before data are acquired. About 25 resonance peaks are recorded at each temperature, which is more than adequate for computing the two independent elastic moduli of a polycrystalline and elastically isotropic material. The above procedure was followed for the *p*-type samples; however, the procedure for *n*-type samples was altered because a feature in the moduli trend was observed near the upper operating range of the direct contact transducers. For these samples, the entire temperature range (300–1250 K) was measured in a continuous fashion with the BR system, eliminating the possibility that any observed shifts in the moduli measurements could be a result of using different data acquisition systems. Once all the resonance spectra were acquired, the resulting spectra at each temperature were fitted by comparing them with computed frequencies. While two of the three sample dimensions can be a free parameter in the fitting process (subject to a constant volume condition), good thermal-expansion data were available for these materials so each dimension was appropriately adjusted at each temperature[4] and dimensions were held constant during the RUS fitting process. Typical RMS errors between observed and computed frequencies are between 0.1–0.3 % over about 25 modes, tending toward the higher end at the higher temperatures due to loading effects and the reduction in the quality factors (increased attenuation).

III. RESULTS AND DISCUSSION

We conducted RUS measurements on both *n*- and *p*-type nanostructured SiGe materials. Young's (E), shear (G), and bulk (B) moduli for the two alloys, derived from both direct contact and buffer rod data, are plotted in Fig. 4. The *p*-type sample shows a modest curvature over the temperature range measured and is fit with a quadratic function (solid line). Measurements were also taken as the sample cooled back to room temperature (not shown) and no hysteresis was observed. A second *p*-type sample was measured upon heating and cooling with results that matched the results shown to within the 1% uncertainty of Young's and bulk moduli (indicated by the error bars). The uncertainty of the shear modulus measurements is about 0.2%. A much stronger dependence of low order mechanical resonances on the shear modulus over extensional or bulk moduli is the root of the higher accuracy.

The *n*-type SiGe shows a different behavior. The moduli decrease linearly until about 650 K where the sample shows an abrupt stiffening. The moduli increase by about 0.5% to a peak at about 800 K, above which a strong quadratic softening is exhibited. Upon cooling, the *n*-type sample does not have the same features, rather the moduli smoothly increase to a slightly stiffer state when it returns to room temperature (open symbols in Fig. 4). The measurements were repeated on a second *n*-type sample which exhibited the same behavior. In this second sample, however, two modifications to the procedure were made: (1) the measurements were made solely with the buffer rod system over the entire temperature range and (2) the sample was reheated after cooling to room temperature. The data upon reheating followed very closely to the previous cooling data indicating that the stiffening feature is a result of a fully irreversible process.

As noted above, these samples are polycrystalline with small crystallites relative to the acoustic wavelengths and as such can be treated as elastically isotropic for which only there are only two independent moduli. The bulk modulus plotted in Fig. 4(c) is derived from the shear and Young's modulus data according to relation $B=EG/(3G-E)$. It is included here for several reasons. First the bulk modulus plays a prominent role in solid state theory (e.g., definition of the Grüneisen parameter and coefficient of thermal expansion). Second, the bulk modulus is easily computed by *ab initio* methods and thus a useful connection between theory and experiment. Third, the bulk modulus is the least sensitive to internal microsctructure of the solid so data for polycrystal-

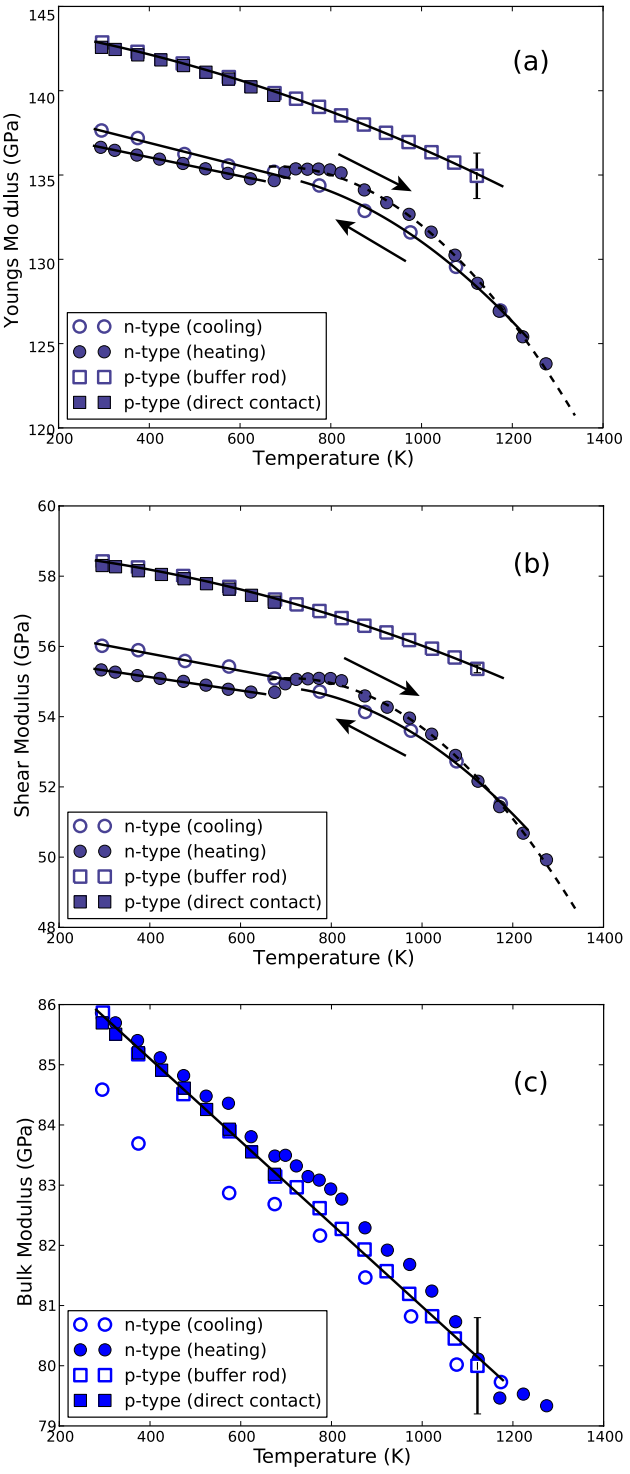

FIG. 4. (Color online) Temperature dependence of (a) Youngs, (b) shear, and (c) bulk moduli of both *n*- and *p*-type SiGe alloys. For the *p*-type samples, filled/open symbols are data obtained with the direct contact/buffer rod systems and the solid line represents a quadratic fit. Note the sharp stiffening of the *n*-type sample beginning at 675 K which does not repeat upon cooling (open circles) or subsequent reheating (not shown). The *n*-type data is fit piecewise: linearly (solid) below 675 K and quadratically (dashed) above. The uncertainty is about 1% in Youngs and bulk moduli (error bars indicated) and 0.2% in the shear modulus (about the size of the symbols).

line and pure crystals are typically comparable. As can be seen from the figure, the bulk modulus for doped nanostructured SiGe is insensitive to both doping types and dopant solubility (more fully described below) which is consistent with the previous statement.

The temperature-dependent stiffening observed for the *n*-type sample appears to be due to the thermally activated phosphorus dopant precipitation in the samples. The solubility limit of phosphorous in SiGe alloys is temperature dependent and appears to reach a maximum value above 1273 K and shows retrograde solubility below 1273 K down to about 600 K.[19] Typical results of electrical resistivity and Seebeck coefficient measurements for *n*- and *p*-type samples are shown in Fig. 5. Note that the curves for the *n*-type samples in these plots have remarkably similar trends to the RUS results and that no hysteresis is observed between heating and cooling curves for the *p*-type samples. Upon heating, the electrical-resistivity values show a sharp increase at about 675 K, which corresponds to the onset of the phosphorous precipitation. When the dopant comes out of solution in SiGe, it presumably precipitates out at the grain boundaries and the fraction of electrically active phosphorous (as a donor) decreases and thus the electrical resistivity increases. At about 800 K, the phosphorus starts to go back into solution and the electrical resistivity decreases up to 1275 K where its solubility is maximal. Upon cooling, the same dopant precipitation is observed and a fraction of the dopant remains precipitated at the grain boundaries all the way down to room temperature. Thus the resulting higher ending value for the electrical resistivity at room temperature.

To further test this hypothesis, the second *n*-type sample was thermally annealed at 1275 K for 30 min and then air quenched to room temperature. This heat treatment ensured that most of the phosphorus redissolved in the SiGe matrix. Repeating the measurements on the reprocessed sample resulted in the same behavior shown in the original measurements in Fig. 4. We believe that this result confirms the temperature-dependent stiffening which is caused by precipitation of dopant atoms. Boron is used as the dopant for *p*-type samples and it does not have a temperature-dependent solubility up to 1100 K, thus the temperature-independent behavior was observed for the moduli of the *p*-type samples.

The stiffening that is observed, concomitant with the phosphorus precipitation, can be attributed to the reduction in the number of Si-P and Ge-P bonds and an increase in the number of Si-Si, Si-Ge, and Ge-Ge bonds. There is support in the literature for the higher stiffness (higher values of elastic constants) for the Si-Si bonds relative to the Si-P bonds. Published data show a significant drop in the elastic constants of silicon in phosphorus-doped silicon relative to the undoped Si matrix whereas no measurable difference was observed between undoped Si and B-doped Si.[20] This would support the hypothesis above that argues for an increase in modulus when phosphorus precipitates out. Additional support for this type of dopant-induced modulus change can be obtained from other systems. An analogous situation was observed in the carbon-nitrogen system.[21] Decreases in the Young's modulus of ultrananocrystalline diamond thin films with increased amounts of nitrogen dopant were attributed to the grain boundary segregation of nitrogen with the attendant

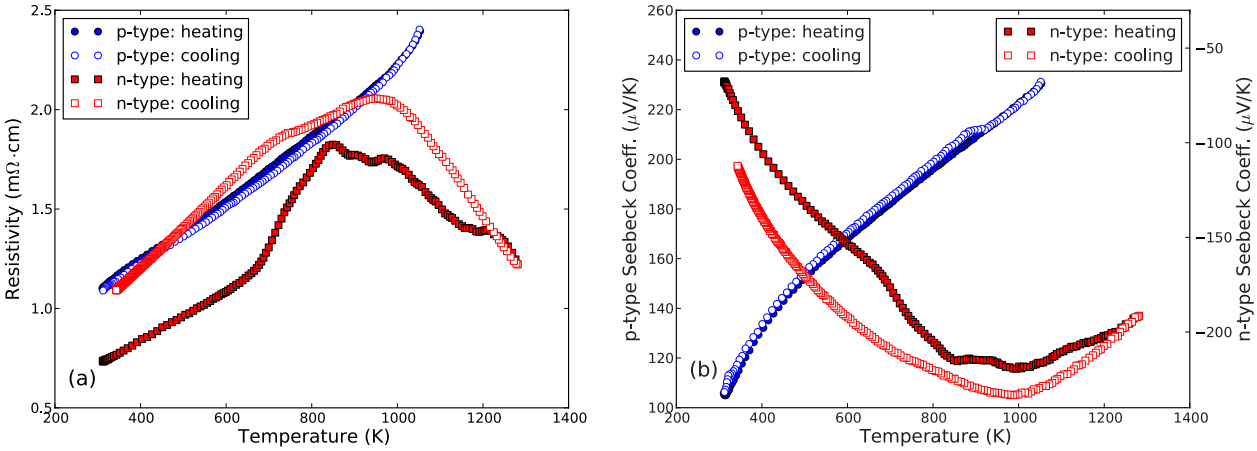

FIG. 5. (Color online) (a) Resistivity and (b) Seebeck coefficient of *n*- and *p*-type SiGe on heating and cooling.

formation of C-N bonds that were compliant relative to the stiff C-C bonds.

Further evidence for the precipitation model comes from an analysis of the acoustic attenuation data. While the center frequencies of the resonance peaks are used to determine elastic moduli, the width of the peaks (Δf) are a measure of attenuation in the material. Absolute acoustic attenuation is difficult to determine from quality factor measurements in a RUS experiment because many factors contribute to energy loss during resonance (transducer loading, small surface defects, acoustic radiation into the heat exchange gas, etc.). However, relative temperature trends of inverse Q measurements, in which changes in the material itself are the dominant factor, can be instructive. Figure 6 shows relative attenuation of both samples as a function of temperature. The relative attenuation is computed by the inverse of the quality factor averaged over all included modes. The general trend shows typical increase in attenuation with an increase in temperature. An interesting feature, however, is observed in the *n*-type sample during heating between 650–800 K where a small but consistent increase in attenuation is exhibited (indicated by the arrow). This is the temperature range of the retrograde phosphorus solubility. It is possible that some of the strain energy of the lattice under resonance is assisting the thermally activated increased solubility of the phosphorous atoms.

IV. CONCLUSIONS

We have presented isotropic elastic moduli measurements of both *n*- and *p*-type nanostructured bulk SiGe at elevated temperatures. The *p*-type samples exhibit smooth softening in the elastic moduli with increasing temperature that fits well with a quadratic function with a slight negative curvature and exhibits no hysteresis. In contrast, the *n*-type samples exhibit a linear softening for temperatures below 675 K, followed by an abrupt stiffening in both Young's and shear moduli of about 0.5% which does not repeat upon cooling or subsequent heating. At higher temperatures the trends exhibit a distinct quadratic curvature. We attribute the stiffening to the precipitation of phosphorus from the Si-Ge matrix upon heating the supersaturated Si-Ge-P solid solution and the corresponding reduction in the number of Si-P and Ge-P bonds. Evidence is cited to support the softening of the elastic constants due to the formation of the Si-P bonds. Supporting experimental evidence is also provided through electrical-resistivity measurements that show similar trends. Thermal treatment of samples to redissolve phosphorus in the matrix demonstrates that the stiffening effect is indeed due to the retrograde solubility of phosphorus in the Si-Ge matrix.

ACKNOWLEDGMENTS

J.R.G. acknowledges the Department of Energy, EPSCoR (Award No. DE-FG02-04ER46121) and NASA (Award No. NM0710850) for support of this project as well as P. Smith for fruitful discussions. Part of this work was carried out at the Jet Propulsion Laboratory, California Institute of Technology, under a contract with the National Aeronautics and Space Administration.

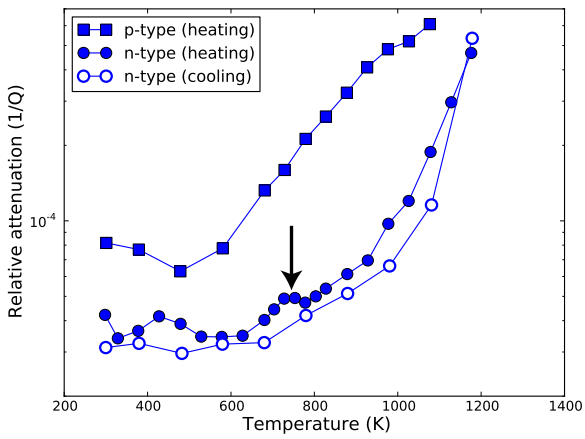

FIG. 6. (Color online) Semilog plot of the relative attenuation of both *n*- and *p*-type SiGe samples as measured by the inverse of the average quality factor ($1/\bar{Q}$) of all included modes for each sample. The arrow highlights an increase in attenuation observed in the *n*-type sample during heating in the retrograde phosphorus solubility region.

[1] S. K. Bux, R. G. Blair, P. K. Gogna, H. Lee, G. Chen, M. S. Dresselhaus, R. B. Kaner, and J.-P. Fleurial, Adv. Funct. Mater. **19**, 2445 (2009).
[2] J. Yang and T. Caillat, MRS Bull. **31**, 224 (2006).
[3] C. B. Vining and J.-P. Fleurial, *A Critical Review of Space Nuclear Power and Propulsion 1984–1993* (AIP, New York, 1994), p. 87.
[4] V. Ravi, S. Firdosy, T. Caillat, E. Brandon, K. van der Walde, L. Maricic, and A. Sayir, J. Electron. Mater. **115**, 38 (2009).
[5] V. Ravi, S. Firdosy, T. Caillat, B. Lerch, A. Calamino, R. Pawlik, M. Nathal, A. Sechrist, J. Buchhalter, and S. Nutt, in *Space Technology and Applications International Forum—STAIF 2008*, edited by M. S. El-Genk (AIP, New York, 2008), Vol. 969, pp. 656–662.
[6] W. M. Visscher, A. Migliori, T. M. Bell, and R. A. Reinert, J. Acoust. Soc. Am. **90**, 2154 (1991).
[7] J. D. Maynard, J. Acoust. Soc. Am. **91**, 1754 (1992).
[8] J. D. Maynard, Phys. Today **49** (1), 26 (1996).
[9] R. G. Leisure and F. A. Willis, J. Phys.: Condens. Matter **9**, 6001 (1997).
[10] A. Migliori, W. M. Visscher, S. Wong, S. E. Brown, I. Tanaka, H. Kojima, and P. B. Allen, Phys. Rev. Lett. **64**, 2458 (1990).
[11] A. Migliori and J. D. Maynard, Rev. Sci. Instrum. **76**, 121301 (2005).
[12] B. Zadler, J. H. L. L. Rousseau, J. A. Scales, and M. L. Smith, Geophys. J. Int. **156**, 154 (2004).
[13] A. Migliori and J. L. Sarrao, *Resonant Ultrasound Spectroscopy: Applications to Physics, Materials Measurements, and Non-Destructive Evaluation* (Wiley, New York, 1997).
[14] T. Goto and O. L. Anderson, Rev. Sci. Instrum. **59**, 1405 (1988).
[15] W. Lins, H. P. G. Kaindl, and K. Kromp, Rev. Sci. Instrum. **70**, 3052 (1999).
[16] ThermoCoax, Inc., www.thermocoax.com
[17] R. Kažys, A. Voleišis, and B. Voleišienė, Ultragarsas (Ultrasound) **63**, 7 (2008).
[18] G. Li, G. A. Lamberton, and J. R. Gladden, J. Appl. Phys. **104**, 033524 (2008).
[19] L. Ekstrom and J. P. Dismukes, J. Phys. Chem. Solids **27**, 857 (1966).
[20] N. Santen and R. Vianden, Mater. Sci. Eng., B **154-155**, 126 (2008).
[21] B. Peng and H. D. Espinosa, in Proceedings of IMECE04, 2004 ASME International Mechanical Engineering Congress, California, 2004 (unpublished), pp. 1–5.